Optimization of angular and frequency compounding in ultrasonic attenuation estimations

Haifeng Tu,[a] James A. Zagzebski, Anthony L. Gerig, Quan Chen, Ernest L. Madsen, and Timothy J. Hall

Department of Medical Physics, University of Wisconsin—Madison, 1300 University Avenue, Room 1530, Madison, Wisconsin 53706

(Received 21 October 2004; revised 31 January 2005; accepted 2 February 2005)

Previous reports have shown that the variance in ultrasound attenuation measurements is reduced when spatial and frequency compounding were applied in data acquisition and analysis. This paper investigates factors affecting the efficiency of compound attenuation imaging methods. A theoretical expression is derived that predicts the correlation between attenuation versus frequency slope (β) estimates as a function of the increment between measurement frequencies (Δf) and the angular separation between beam lines ($\Delta\theta$). Theoretical results are compared with those from attenuation measurements on tissue-mimicking phantoms and from simulation data. Both predictions and measurement results show that the correlation between β estimates as a function of (Δf) is independent of the length of the radio frequency (rf) data segment over which β is derived. However, it decreases with an increase in the length of the data segment used in power spectra estimates. In contrast, the correlation between β estimates as a function of $\Delta\theta$ decreases when the rf data segment length is longer or the frequency of the signal is higher. © *2005 Acoustical Society of America.* [DOI: 10.1121/1.1879212]

PACS numbers: 43.80.Vj, 43.80.Qf [FD] Pages: 3307–3318

LIST OF SYMBOLS

α	attenuation coefficient (dB/cm)
α_{f_i}	attenuation coefficient at frequency f_i
a_m	coefficient related with least square process
β	attenuation coefficient versus frequency slope ($\beta=\alpha/f$)
β''	attenuation coefficient versus frequency slope after spatial and frequency compounding
β_{f_i}	attenuation coefficient versus frequency slope at frequency f_i ($\beta_{f_i}=\alpha_{f_i}/f_i$)
$\beta_{\theta_i}(f_k)$	attenuation coefficient versus frequency slope at angle θ_i and frequency f_k
β_{θ_i}	attenuation coefficient versus frequency slope at angle θ_i, $\beta_{\theta_i}=\Sigma_{k=1}^{n_f}\beta_{\theta_i}(f_k)/n_f$
b	distance between the center of apertures
BSC	backscatter coefficient
$\mathrm{cov}(\beta_{f_i},\beta_{f_j})$	covariance between β_{f_i} and β_{f_j}
D	aperture
f	frequency
Δf	frequency separation between successive frequencies at which β values are calculated
θ	the angle between the beam axes
φ	the half angle between the beam axes
k	inverse of signal-to-noise ratio SNR ($k=1/\mathrm{SNR}$)
$l_{\min}$	minimum gating coordinate
$l_{\max}$	maximum gating coordinate
m	spatial index of independent power spectra estimate involved in α derivation
n	the number of independent power spectra estimates over Z
n_c	the number of partially correlated angular beam lines
n_f	the number of partially correlated frequency components
N	the number of independent A-lines used in power spectra estimates
N_c	the effective number of independent angular beam lines
N_f	the effective number of independent frequency components
$\sigma_{\alpha_{f_i}}$	standard deviation of α_{f_i}
$\sigma_{\beta_{f_i}}$	standard deviation of β_{f_i}
$\sigma_{\beta_{\theta_i}(f_k)}$	standard deviation of $\beta_{\theta_i}(f_k)$
σ''_β	standard deviation of β after spatial and frequency compounding
$\rho(\beta_{f_i},\beta_{f_j})$	correlation between β_{f_i} and β_{f_j}
$\rho(\beta_{\theta_i},\beta_{\theta_j})$	correlation between β_{θ_i} and β_{θ_j}
$\rho(\beta_{\theta_i}(f_k),\beta_{\theta_j}(f_k))$	correlation between $\beta_{\theta_i}(f_k)$ and $\beta_{\theta_j}(f_k)$
S_{f_i}	periodogram spectral estimate at frequencies f_i
$S_{f_i}^m$	mth periodogram spectral estimate at frequencies f_i
$S_{\theta_i}(f_k)$	periodogram spectral estimate at angles θ_i and frequency f_k
$S_{\theta_i}^m(f_k)$	mth periodogram spectral estimate at angles θ_i and frequency f_k
$\rho(S_{f_i},S_{f_j})$	correlation between S_{f_i} and S_{f_j}

[a]Electronic mail: htu@wisc.edu

$\rho(S^m_{f_i}, S^m_{f_j})$	correlation between $S^m_{f_i}$ and $S^m_{f_j}$
$\rho(S_{\theta_i}(f_k), S_{\theta_j}(f_k))$	correlation between $S_{\theta_i}(f_k)$ and $S_{\theta_j}(f_k)$
$\rho_{1,2}(f_k)$	correlation between Fourier transformed segments whose squared modulus is $\rho(S_{\theta_i}(f_k), S_{\theta_j}(f_k))$
$\rho(S^m_{\theta_i}(f_k), S^m_{\theta_j}(f_k))$	correlation between $S^m_{\theta_i}(f_k)$ and $S^m_{\theta_j}(f_k)$
RS	ratio of power spectra from the sample to the reference
S	power spectra
T	length of gating window applied in power spectra estimates
$p(t)$	gating window applied in periodogram spectral estimates
$p(x,y,f)$	point spread function at frequency f
z	depth
z_0	focal distance
Z	length of the rf data segment over which a value of β is computed
λ	wavelength
$\Delta\Omega_{1,2}$	volume for integration

I. INTRODUCTION

Objectively determined ultrasound attenuation values in tissues could provide useful information about disease in various sites, including the liver,[1,2] breast,[3,4] myocardium,[5] and human aorta.[6] Many methods based on pulse echo techniques have been proposed for estimating the attenuation coefficient. In general, they can be classified as either time domain methods[7–10] or frequency domain methods.[11–14]

Except for work by Walach *et al.*, determination of such values in small, localized regions identified on ultrasound B-mode images or the production of attenuation images are rarely reported. This is partially because of the requirement for large data segments to achieve statistically precise results. We have reported a method[15] which effectively decreases variance in attenuation estimations made over small volumes of tissue. The method uses spatial angular and frequency compounding in the data acquisition and analysis. A reference phantom is applied to account for imaging system dependencies of echo signals. Results demonstrate an effective reduction of the variance in attenuation versus frequency slope ($\beta = \alpha/f$) measurements when compounding is applied versus when no compounding is used. Low-frequency attenuation images of a 3-cm-diam cylinder with 0.3-dB/cm/MHz β contrast in a phantom demonstrated the accuracy and precision of this technique.[15]

In this paper, we further investigate factors affecting the efficiency of spatial angular and frequency compounding through studies of variance reduction in attenuation estimations. A theoretical expression is derived that predicts the correlation between β estimates as a function of the increment between measurement frequencies and the angular separation between beam lines. Theoretical results are compared with those from β measurements on tissue mimicking phantoms using beam steering with a linear array and from simulation data computed for situations where a transducer rotates around its transmit focus. Various factors affecting the decorrelation rate are discussed. The results can be used to optimize spatial angular and frequency compounding schemes in attenuation versus frequency slope derivations.

II. THEORY

A. The reference phantom method (RPM)

The reference phantom method developed by Yao *et al.*[13] is used for attenuation and backscatter estimations. In this method, the echo signal intensity from a sample is compared to the signal intensity at the same depth from a reference phantom, whose attenuation and backscatter properties are known. The reference phantom data are acquired using the same transducer and system settings used for acquiring echo data from the sample. For a gated radio frequency (rf) signal, $\mathrm{RS}(f,z)$, the ratio of the power spectrum from the sample to that from the reference at frequency f and depth z can be expressed as[13]

$$\mathrm{RS}(f,z) = \frac{S_s(f,z)}{S_r(f,z)} = \frac{\mathrm{BSC}_s(f)}{\mathrm{BSC}_r(f)} e^{-4(\alpha_s(f)-\alpha_r(f))z}, \tag{1}$$

where the S's are power spectra; subscripts s and r refer to the sample and reference, respectively; the BSCs are backscatter coefficients; and α's are sample and reference phantom attenuation coefficients at f.

After a least squares line-fit of the curve $\ln(\mathrm{RS}(f,z))$ versus depth, z, the slope is proportional to the difference between the sample and reference attenuation coefficients. Since the latter is known, this provides the attenuation coefficient of the sample. For a uniform sample, the zero depth intercept yields the ratio of the sample and reference backscatter coefficients.

Assume the attenuation in the sample is linearly proportional to the frequency, which is approximately true in tissue for frequencies in the range of 1 to 10 MHz. Thus,

$$\alpha(f) = \beta f. \tag{2}$$

The attenuation coefficient versus frequency slope, β (dB/cm/MHz), is a useful attenuation parameter, and it will be used throughout our study.

B. Role of spatial angular and frequency compounding

Local attenuation estimations are limited by the large variance due to the presence of statistical fluctuations in the backscattered signals. An analysis of the statistical uncertainty of attenuation values derived using the reference phantom method has been presented by Yao *et al.*[16] Generally, the power spectra in Eq. (1) are estimated using data from multiple beam lines acquired from the sample and the reference. The standard deviation of the attenuation coefficient at frequency f_i, $\sigma_{\alpha_{f_i}}$, is related to the uncertainty of the slope

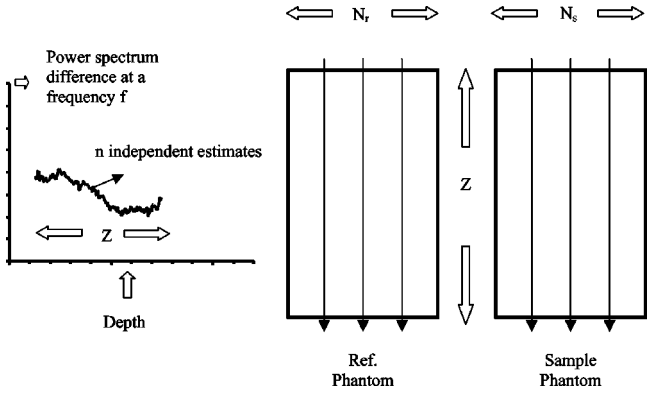

FIG. 1. Data acquisition and processing using a reference phantom to determine attenuation over a region whose axial length is Z. Independent echo signal segments from N_s beam lines in the sample and N_r beam lines in the reference are involved. Adapted from Ref. 15.

calculation of $\ln(\mathrm{RS}(f,z))$ vs. z when the measured values exhibit statistical fluctuations. Results show that $\sigma_{\alpha_{f_i}}$ is given by (see Fig. 1)

$$\sigma_{\alpha_{f_i}} = \frac{7.52k\sqrt{N_s+N_r}}{\sqrt{(n+1)/(n-1)}\sqrt{n}Z\sqrt{N_sN_r}}\,(\mathrm{dB/cm}), \tag{3}$$

where N_r and N_s are the number of independent acoustical lines over which echo data are acquired and analyzed from the reference and the sample, respectively; Z is the length of the rf data segment over which the least squares analysis is applied; n is the number of independent power spectral estimates over the interval Z ($n \geqslant 3$); and the factor k is the inverse of the ''signal-to-noise ratio,'' that is, the mean of the signal intensity to its standard deviation. This ratio is 1 if Rayleigh statistics apply.[17] Since n is proportional to Z, the uncertainty is inversely proportional to the $\frac{3}{2}$ power of the length of the data segments for large n. This expression is different from Yao's original expression because here independent power spectral estimates are modeled as discrete, uniformly spaced data points instead of continuous data points.

One means to decrease the uncertainty in attenuation coefficient estimations without excessively expanding the region over which the estimation is done is to apply spatial angular compounding. Spatial angular compounding during echo data acquisition has proven to be an effective technique for reducing speckle noise to improve B-mode image quality.[18] The method has only recently been used to improve quantitative ultrasound images.[15,19] Another method to decrease errors in these estimations is to average attenuation coefficients derived from different frequency components of the echo signal spectrum. This technique called ''frequency compounding'' has also been applied to reduce speckle in ultrasound images.[20,21] In the case of attenuation imaging, it has been found advantageous to apply frequency compounding in estimations of β, the attenuation coefficient versus frequency slope defined in Eq. (2).[15]

The statistical uncertainty of estimations of the attenuation coefficient versus frequency slope (β) when both spatial and frequency compounding are applied can be described using the following expression:[15]

$$\sigma''_{\beta} = \frac{1}{\sqrt{N_c}} \cdot \frac{1}{N_f} \cdot \sqrt{\sum_{i=1}^{n_f} \sigma^2_{\beta_{f_i}}}, \tag{4}$$

where σ''_{β} is the standard deviation of the attenuation coefficient versus frequency slope β'', after spatial angular and frequency compounding, and $\sigma_{\beta_{f_i}}$ is the standard deviation of β at frequency f_i, given by $\sigma_{\beta_{f_i}} = (1/f_i)\,\sigma_{\alpha_{f_i}}$. N_f in Eq. (4) is the effective number of independent frequency components used in the attenuation versus frequency slope estimation, and N_c is the effective number[22] of independent beam lines used for spatial angular compounding. n_f is the number of compounded frequency components, which may be partially correlated.

As shown by Eq. (4), increasing N_f or N_c promotes lower standard deviations. Thus, effective use of the signal frequency bandwidth as well as the angular window available for compounding requires knowledge of correlations amongst frequency and amongst angular estimates. With this information, it would be possible to increase the frequency separation between chosen frequency components, as well as the angular separation among the selected beam lines, so that near maximum reduction in σ''_{β} can be achieved using a relatively small number of frequency components or angular beam lines, saving time in data acquisition and processing. Sec. II C 3 outlines a theory that predicts these correlations.

C. Attenuation estimate correlation

1. Correlation between β estimates as a function of the increment between measurement frequencies

Suppose n_f is the total number of (partially correlated) frequency components compounded. Thus, N_f, the effective number of independent frequency components is associated with n_f, the actual number of frequency components used, through the following relation,[15]

$$N_f = \frac{n_f}{\sqrt{1+(\Sigma_{i\neq j}^{n_f}\sigma_{\beta_{f_i}}\sigma_{\beta_{f_j}}\rho(\beta_{f_i},\beta_{f_j}))/\Sigma_{i=1}^{n_f}\sigma^2_{\beta_{f_i}}}} = \frac{n_f}{\delta}, \tag{5}$$

where, $\sigma^2_{\beta_{f_i}}$ is the variance of the attenuation versus frequency slope estimate at frequency f_i, $\delta = \sqrt{1+(\Sigma_{i\neq j}^{n_f}\sigma_{\beta_{f_i}}\sigma_{\beta_{f_j}}\rho(\beta_{f_i},\beta_{f_j}))/\Sigma_{i=1}^{n_f}\sigma^2_{\beta_{f_i}}}$, and $\rho(\beta_{f_i},\beta_{f_j})$ is the correlation between the attenuation versus frequency slopes, estimated at frequencies f_i and f_j. Knowledge of $\rho(\beta_{f_i},\beta_{f_j})$ is the key to increasing the efficiency of frequency compounding in attenuation variance reduction.

Since β is derived from power spectral estimates, it is natural to look for $\rho(\beta_{f_i},\beta_{f_j})$ through the correlation between spectral estimates at frequencies f_i and f_j. We have developed a theory that approximates $\rho(S_{f_i},S_{f_j})$, the correlation between periodogram spectral estimates at any two frequencies, f_i and f_j (see Appendix A). This is given by

$$\rho(S_{f_i},S_{f_j}) = |FT(|p(t)|^2)_{\Delta f}|^2, \tag{6}$$

where $p(t)$ is a gating window applied to the rf data in the periodogram spectral estimates, and $\Delta f = |f_j - f_i|$. Thus $\rho(S_{f_i}, S_{f_j})$ only depends on Δf and the length of the gating window T.

It is possible to derive $\rho(\beta_{f_i}, \beta_{f_j})$ from $\rho(S_{f_i}, S_{f_j})$, and this will be described in Sec. II C 3.

2. Correlation between β estimates as a function of the angular separation between beam lines

N_c, the effective number of independent signals used for spatial angular compounding, can be associated with n_c, the actual number of angular signals used, through the following relation:

$$\frac{1}{N_c} = \frac{1}{n_c} + \sum_{i \neq j}^{n_c} \rho(\beta_{\theta_i}, \beta_{\theta_j}) \tag{7}$$

where $\rho(\beta_{\theta_i}, \beta_{\theta_j})$ is the correlation between attenuation coefficient versus frequency slopes β_{θ_i}, β_{θ_j} at two angular positions θ_i and θ_j $(i \neq j)$, derived after frequency compounding.[15] $(\beta_\theta = (\Sigma_{k=1}^{n_f} \beta_\theta(f_k))/n_f$, where $\beta_\theta(f_k)$ is the attenuation versus frequency slope estimated at angle θ and frequency f_k. The geometry is illustrated in Fig. 2. This correlation can be estimated as (see Appendix B)

$$\rho(\beta_{\theta_i}, \beta_{\theta_j}) = \frac{\sum_{k=1}^{n_f} (1/f_k^2)\, \rho(\beta_{\theta_i}(f_k), \beta_{\theta_j}(f_k))}{\delta^2 \sum_{k=1}^{n_f} (1/f_k^2)}, \tag{8}$$

where f_k is the kth frequency component used in frequency compounding and δ was defined previously. Therefore, $\rho(\beta_{\theta_i}(f_k), \beta_{\theta_j}(f_k))$, the correlation between attenuation coefficient versus frequency slopes, estimated at angles θ_i and θ_j for frequency f_k, is the critical information needed to increase the efficiency of spatial angular compounding in attenuation variance reduction.

To derive $\rho(\beta_{\theta_i}(f_k), \beta_{\theta_j}(f_k))$, we start with the correlation between power spectral estimates at angular position θ_i and θ_j, and at frequency f_k. Gerig and Chen[23] describe a model for the correlation between periodogram spectral estimates for rf data acquired at angular positions θ_i and θ_j (see Fig. 2). In this setup, positions 1 and 2 are locations of an aperture interrogating the same region but from different angles. The region is assumed to be centered at the focal

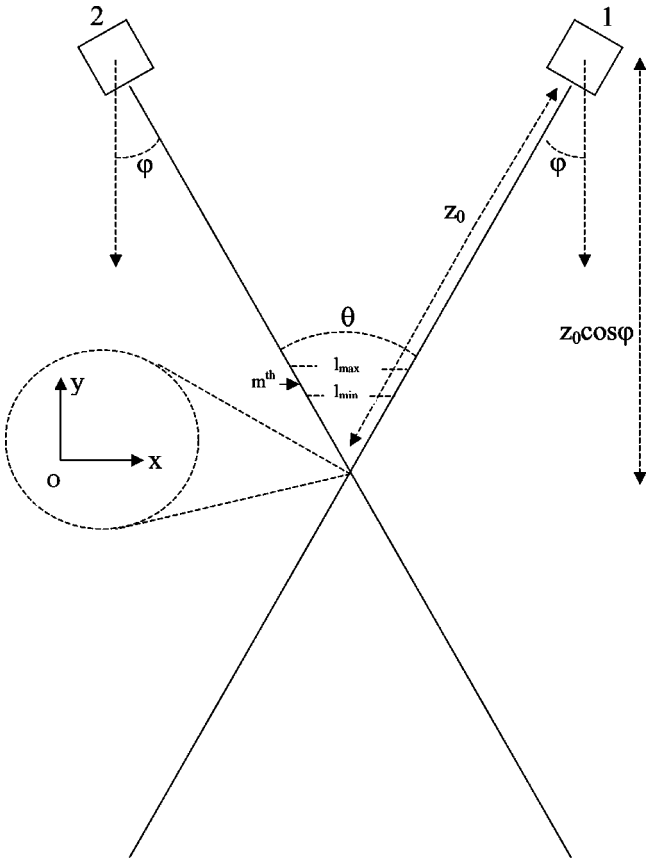

FIG. 2. The coordinate system used in deriving the spectral correlation between rf data from angled beam lines. Adapted from Ref. 23.

distance, z_0, which will be taken as the origin of the coordinate system. θ is the angle between the beam axes, and φ is its half angle; b is the distance between the centers of the apertures, which is also given by $b = 2z_0 \sin\varphi$. $\Delta\Omega_{1,2}$ is the volume contributing to the echo data, where the x direction extends to the edges of the beam and the y direction is bounded by the position and length of the rf data segment. Then, $\rho(S_{\theta_i}(f_k), S_{\theta_j}(f_k))$, the correlation between periodogram spectral estimates at angular position θ_i and θ_j for frequency f_k, is[23]

$$\rho(S_{\theta_i}(f_k), S_{\theta_j}(f_k)) = |\rho_{1,2}(f_k)|^2, \tag{9}$$

where $\rho_{1,2}(f_k)$ is the corresponding correlation between Fourier transformed segments. The latter can be written as

$$\rho_{1,2}(f_k) \approx \frac{\int_{\Delta\Omega_{1,2}} dx\,dy\,p(x\cos\varphi - y\sin\varphi, x\sin\varphi + y\cos\varphi, f_k)\, p(x\cos\varphi + y\sin\varphi, -x\sin\varphi + y\cos\varphi, f_k)}{\int_{\Delta\Omega_{1,2}} dx\,dy\,p^2(x,y,f_k)}$$
$$\times \frac{e^{2ik\left(\sqrt{(x-b/2)^2 + (z_0\cos\varphi - y)^2} - \sqrt{(x+b/2)^2 + (z_0\cos\varphi - y)^2}\right)} \{1/[(x-b/2)^2 + (z_0\cos\varphi - y)^2]\, 1/[(x+b/2)^2 + (z_0\cos\varphi - y)^2]\}}{1/[x^2 + (z_0 - y)^2]^2}. \tag{10}$$

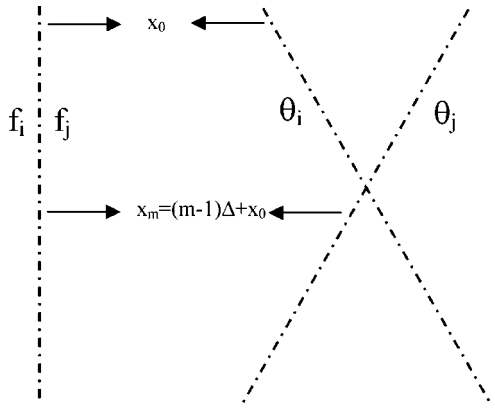

FIG. 3. Sketches to help illustrate derivation of Eqs. (11) and (12) in Appendix C. Dots stand for independent spectral estimate points. The left panel depicts the situation in Eq. (11), while the right panel is for Eq. (12).

In this expression, $p(x,y,f)$ is the point spread function, with $\varphi=\theta/2=|\theta_j-\theta_i|/2$. [Gerig *et al.* use ω in place of f_k. They use subscripts 1 and 2 for θ_i and θ_j, and they use $\rho_s(\omega)$ rather than $\rho(S_{\theta_i}(f_k),S_{\theta_j}(f_k))$.]

Similar to Sec. C II 1, it is possible to associate $\rho(\beta_{\theta_i}(f_k),\beta_{\theta_j}(f_k))$ with $\rho(S_{\theta_i}(f_k),S_{\theta_j}(f_k))$, which is the correlation between periodogram spectral estimates at angular positions θ_i and θ_j at frequency f_k. This will be explained in the next section.

3. Relation between attenuation versus frequency slope correlations and correlation among rf signal power spectra

The efficiency of compounding in attenuation variance reduction depends on the correlation between β estimates as a function of (1) the increment between analysis frequencies, $\rho(\beta_{f_i},\beta_{f_j})$, and (2) the angular separation between beam lines, $\rho(\beta_{\theta_i}(f_k),\beta_{\theta_j}(f_k))$.

Regardless of whether the problem involves correlations between the attenuation versus frequency slope at two frequencies (for a fixed angle) or at two angular positions (for a fixed frequency), it is essentially the same problem associating an attenuation correlation with a corresponding power spectra correlation. That is, the correlation between the attenuation versus frequency slope at positions 1 and 2 can be associated with the power spectra correlation at these positions through a common process, be it for two frequencies or two spatial angular positions (see Appendix C and Fig. 3). Let $\rho(S_{f_i},S_{f_j})$ be the correlation between sample power spectral estimates at frequencies f_i and f_j, and let $\rho(S_{\theta_i}(f_k),S_{\theta_j}(f_k))$ be the correlation of the same quantity as a function of the angular separation between beam lines. This is expressed by the following equations:

$$\rho(\beta_{f_i},\beta_{f_j})=\frac{12}{(n-1)n(n+1)}\sum_{m=1}^{n}a_m^2\rho(S_{f_i}^m,S_{f_j}^m) \tag{11}$$

and

$$\rho(\beta_{\theta_i}(f_k),\beta_{\theta_j}(f_k))=\frac{12}{(n-1)n(n+1)}\sum_{m=1}^{n}a_m^2\rho(S_{\theta_i}^m(f_k),S_{\theta_j}^m(f_k)) \tag{12}$$

where $a_m=m-n/2-\frac{1}{2}$ and $\Sigma_{m=1}^{n}a_m^2=(n-1)n(n+1)/12$ if the attenuation coefficient over region Z is obtained using a least squares method to derive the slope of the log of the power spectrum versus depth. m is a spatial index designating independent power spectral estimates at different depths, and n is the total number of independent estimates within Z, the same as in Eq. (3) (see Appendix C).

It is clear that $\rho(S_{f_i},S_{f_j})$ only depends on Δf and the length of the window T, and it is independent of the index m. Thus, $\rho(\beta_{f_i},\beta_{f_j})$, the correlation between attenuation coefficient versus frequency slopes estimated at two frequencies f_i and f_j, is obtained from

$$\rho(\beta_{f_i},\beta_{f_j})=\rho(S_{f_i},S_{f_j})\frac{12}{(n-1)n(n+1)}\sum_{m=1}^{n}a_m^2$$
$$=\rho(S_{f_i},S_{f_j})=|FT(|p(t)|^2)_{\Delta f}|^2. \tag{13}$$

$\rho(S_{\theta_i}^m(f_k),S_{\theta_j}^m(f_k))$ can be derived from Eqs. (9) and (10), by integrating in the region $\Delta\Omega_{1,2}^m$ where echo data for the mth corresponding periodogram spectral estimate originate. Therefore, $\rho(\beta_{\theta_i}(f_k),\beta_{\theta_j}(f_k))$ can be estimated from Eq. (12) with the knowledge of $\rho(S_{\theta_i}^m(f_k),S_{\theta_j}^m(f_k))$.

III. METHOD

A. Correlation between β estimates as a function of the increment between measurement frequencies

To test Eq. (13), a uniform phantom with 0.5 dB/cm/MHz attenuation was used. The same phantom was used both as a sample and a reference by scanning different regions to assure independent data. A VFX13-5 linear array transducer on a Siemens Antares scanner (Siemens Medical Solutions, Ultrasound Division, Mountain View, CA, USA) was used to acquire the data. A single transmit focus set at a depth of 3 cm was used. The scanner is equipped with a research interface, providing raw beam line data in a radio frequency format as well as header data indicating beam position, frequency, etc. The sampling frequency was 40 MHz, and the line density was 50 lines/cm.

Eleven rf data sets, each consisting a frame of echo data across the entire field of view of the probe, were acquired. The number of acoustic lines acquired in each frame is 192. The transducer was translated in the elevational direction between sets. The translation step was larger than the elevational dimension of the transducer, so that all rf data sets can be regarded as independent because different portions of the phantom were isonified. One data set served as a reference, and the remaining ten sets were taken as samples.

Analysis was done by computing the attenuation coefficient versus frequency slope for segments of individual beam lines whose length, Z, was either 2.16 or 2.77 cm, centered at the 3-cm transmit focal depth. Echo data from within each segment were first divided into subsegments defined by 4-μs

rectangular gating windows (3 mm), with no overlap. For each window, the spectrum was computed by taking the Fourier transform. A rectangular window with no overlap ensured accurate gating of the rf data and independence of power spectral estimates over the segment, as required in our theoretical analysis. Then, Eq. (13) changes to

$$\rho(\beta_{f_i},\beta_{f_j})=\mathrm{sinc}^2(T\Delta f), \tag{14}$$

where T is 4 μs and $\Delta f=|f_j-f_i|$.

In the case of the data from the reference, power spectral values at a given measurement depth were averaged over all 192 beam lines to provide a reference spectra at each depth, with low variability. $\alpha(f)$ was then calculated for each segment by fitting a straight line to the spectral values versus depth, as discussed after Eq. (1). Then attenuation versus frequency slopes ($\beta=\alpha/f$) at frequencies over a range from 6 to 14 MHz were calculated for the segment. One hundred ninety-two such parallel segments from the sample were available for each rf data set.

Correlation between β as a function of the increment between measurement frequencies was calculated for each rf data set using the following formula:

$$\text{Correlation}=\frac{\langle[\beta_{f_i}-\text{mean}(\beta_{f_i})]\cdot[\beta_{f_j}-\text{mean}(\beta_{f_j})]\rangle}{\sigma_{\beta_{f_i}}\cdot\sigma_{\beta_{f_j}}}, \tag{15}$$

where, as defined before, β_{f_i} is the attenuation coefficient versus frequency slope at frequency f_i, and β_{f_j} is the same quantity evaluated at frequency f_j. There are 192 pairs of β_{f_i}, and β_{f_j} for each sample rf data set. Mean (β_{f_i}) and mean (β_{f_j}) are their mean values, and $\sigma_{\beta_{f_i}}$, $\sigma_{\beta_{f_j}}$ are their standard deviations; here $\langle ... \rangle$ stands for the expected value.

Correlation values from frequency pairs that have the same frequency separation, Δf, were averaged to get final correlation values for one independent sample rf data set. In the end, the mean values of these ten independent correlation results from the ten rf data sets were taken as the experimental values, and error bars were calculated by calculating the standard deviation. Theoretical values were obtained from Eq. (14).

B. Correlation between β estimates as a function of the angular separation between beam lines

The accuracy of Eq. (12) was explored using simulated data because key information, including the dynamic aperture of transducers on the scanner, was not available and because simulation code can provide ideal rf data at specified beam angles. Using a simulation program,[25] rf echo signals were modeled for a linear array transducer interrogating a medium containing randomly distributed scatterers. The scatterer size of polystyrene beads applied in the simulation was 50 μm, and the scatterer number density was 9.7 per cubic millimeter, assuring that Rayleigh statistics apply. The linear array consists of elements of size 0.15 mm by 10 mm, with a center-to-center distance of 0.2 mm. Signals for each beam line were assumed to be formed using rf echo data from 75 consecutive elements, for a 1.5-cm aperture. Each of ten independent sample data sets simulated contained 180 lines, with each beam line rotated 0.5° from the previous, yielding a minimum angle of 0° and a maximum of 89.5° between pairs of beam lines. The focus was set at 3 cm from the transducer surface. A reference data set was also simulated, containing 400 lines. The power spectra at each depth within this set were averaged to provide reference spectra. For convenience, the attenuation of the sample was set to be zero while the reference attenuation was assumed in the model to be 0.5 dB/cm/MHz. The speed of sound in both media was set to be 1540 m/s. Neither apodization, dynamic receive focus, nor dynamic aperture were used.

Assume, for the sake of simplicity, the point-spread function for the system is adequately represented by a sinc squared function and the amplitude of the field does not vary significantly near the transmit focus. Equation 10 changes to

$$\rho_{1,2}(f_k)\approx\frac{\int_{\Delta\Omega_{1,2}}dxdy\ \mathrm{sinc}^2[(D/z_0\lambda)\,(x\cos\varphi-y\sin\varphi)]\mathrm{sinc}^2[(D/z_0\lambda)\,(x\cos\varphi+y\sin\varphi)]e^{2ik(\sqrt{(x-b/2)^2+(z_0\cos\varphi-y)^2}-\sqrt{(x+b/2)^2+(z_0\cos\varphi-y)^2})}}{\int_{\Delta\Omega_{1,2}}dxdy\ \mathrm{sinc}^4(Dx/z_0\lambda)}. \tag{16}$$

To derive $\rho(S^m_{\theta_i}(f_k),S^m_{\theta_j}(f_k))$ so that Eq. (12) can be solved, integration in Eq. (16) has to be made in the region $\Delta\Omega^m_{1,2}$ where scatterers contributing to the mth corresponding periodogram spectral estimate exist. The integration limits in the y direction were approximated roughly by setting them according to the coordinate along the y axis: $y_{\min}=l_{\min}\cos\varphi$ and $y_{\max}=l_{\max}\cos\varphi$. $l_{\min}$ is the minimum rectangular gating coordinate of the mth subsegment along the beam line, while $l_{\max}$ is the maximum gating coordinate (see Fig. 2). As in Sec. C 1, a 4-μs rectangular gating window (3 mm) with no overlap was used in the periodogram spectral estimates. In addition, as mentioned before, integration in the x direction was bounded by the edges of the beam.

For frequency f_k, attenuation coefficient versus frequency slopes over a specified region of each angled beam line were computed. Not losing generality, segments of each line, centered at the focus, were chosen as these regions. Correlation between attenuation versus frequency slope estimates as a function of the angular separation between beam lines was obtained for each of the ten independent sample data sets in a similar manner as described in Eq. (15). The difference is that in this case $\beta_{\theta_i}(f_k)$ and $\beta_{\theta_j}(f_k)$, the attenuation coefficient versus frequency slopes estimated at angles θ_i and θ_j for frequency f_k, replace β_{f_i} and β_{f_j} in Eq. (15). Their standard deviations $\sigma_{\beta_{\theta_i}(f_k)}$ and $\sigma_{\beta_{\theta_i}(f_k)}$ replace $\sigma_{\beta_{f_i}}$ and $\sigma_{\beta_{f_j}}$ in the same equation. The mean value of these ten independent correlation results from the ten independent

sample data sets was calculated. Theoretical values were obtained from Eq. (12).

IV. RESULTS

A. Correlation between β estimates as a function of the increment between measurement frequencies: Measurement data

Correlations between β estimates as a function of the increment between measurement frequencies (Δf) were calculated for rf data segments of length 2.16 and 2.77 cm. Results are shown in Figs. 4(a). (2.16 cm) and (b) (2.77 cm). Here experimental values are labeled as dots with error bars, while theoretical values calculated using Eq. (14) are plotted as solid lines. Error bars display $\pm$ one standard deviation of the ten independent correlation estimates in each case. For both data segment lengths, experimental values appear to match well with theoretical values in the general trend, although discrepancies are noted in the magnitude of the decorrelation rate. These are discussed in Sec. V. Both experimental and theoretical results indicate that the data segment length is not a factor in the correlation between β estimates at different measurement frequencies. An approximate 0.2-MHz increment between frequencies at which β results are obtained yields completely uncorrelated data when the length of the gating window used, T, is 4 μs.

B. Correlation between β estimates as a function of the angular separation between beam lines: Simulated data

Correlations between attenuation versus frequency slopes at different beam angles were computed for simulated data derived using center frequencies of 3, 5, and 7 MHz. In each case, a 50% bandwidth was represented in the simulation. For each simulated data set, the correlation between β values estimated at different angular separations between beam lines ($\Delta\theta$) was obtained for both 2.16- and 2.77-cm rf data segments. Results are shown in Fig. 5 (2.16 cm) and Fig. 6 (2.77 cm) for the three different center frequencies. Values from simulations are labeled as dots with error bars, while theoretical values are plotted as solid lines. Again, error bars display $\pm$ one standard deviation of the ten independent correlation estimates in each situation. In all situations, the agreement in the general trend between experimental values and theoretical values is good; i.e., it can be seen from both simulation data and theory that the higher the frequency is, the faster is the decorrelation between β estimates as a function of the angular separation between beam lines. A similar statement can be made regarding the effect of data length, namely, attenuation computed over longer segments decorrelates faster with angle. For the situation simulated at 3.5 MHz, the angular increment needed for the attenuation estimates to achieve 0.5 decorrelation is around 2° for the 2.16-cm data segment and 1.6° for the 2.77-cm segment. At 5 MHz, the values are 1.5° for 2.16 cm and 1.2° for 2.77 cm, while at 7 MHz, they are 1.1° for 2.16-cm segments and 0.8° for 2.77-cm segments.

V. DISCUSSION

The theoretical expressions derived in this paper predict the correlation between β estimates as a function of increment between measurement frequencies and angular separation between beam lines. Predictions are found to match experimental results in the general trend of the curves, as noted in the results. However, small deviations between predictions and measurement results are also noticed in Figs. 4–6. Part of the deviation may be contributed by the error propagation assumption used in deriving the theoretical expressions. We associated the covariance of the sample-to-reference power spectrum ratio with the covariance of its logarithm form [Appendix C, Eqs. (C8) and (C12)] in an approximate partial derivative relation. Nevertheless, these theoretical curves give a good approximation to the decorrelation rate in attenuation estimations for incremental changes in beam angle and analysis frequency.

In the frequency compounding method, from Eq. (14), the correlation between β estimates as a function of increment between measurement frequencies is dependent on the length of the gating window, T. The longer T is, the more independent frequency components there are within the bandwidth of the transducer, making N_f in Eq. (4) larger. On the other hand, the longer T is, the smaller will be n, the number of independent spectral estimates over the interval Z, tending to make $\sigma_{\beta_{f_i}}$ in Eq. (4) larger because $\sigma_{\alpha_{f_i}}$ would be larger [see Eq. (3)]. Therefore, according to Eq. (4), there is no apparent difference in terms of reducing the variance of β between long or short gating windows, for the power spectra estimates, provided that the length of the gating window is long enough to make stable attenuation estimates at different frequencies over the spectrum. Yao[26] pointed out that for a Blackman-Harris window, 4 μs is needed for stable attenuation estimates around 5 MHz. Also, because the correlation between β estimates as a function of increment between measurement frequencies is independent of the length of the rf data segment over which attenuation is computed, frequency compounding will have an advantage in local attenuation estimations where data lengths are short.

In angular compounding, the correlation between β estimates as a function of angular separation between beam lines is dependent on both the frequency of the signal and the length of the rf data segment over which the attenuation value is derived. Figures 5 and 6 illustrate that the higher the frequency or the longer the data segment is, the faster the decorrelation with beam angle is. Thus it is a good strategy to include more high-frequency components to get more independent angular estimates, as shown by Eq. (8). The effect of data length on the decorrelation between β estimates puts an adverse effect on attempts to improve resolution in local attenuation estimations where it would be desirable to keep data lengths short. The efficacy of angular compounding in variance reduction of attenuation estimations is limited due to this effect.

To verify Eq. (12), the point spread function was taken to behave as a sinc-squared function, and the field amplitude was assumed to vary insignificantly for sample data sets near the transmit focus, so that the calculation of Eq. (10) could

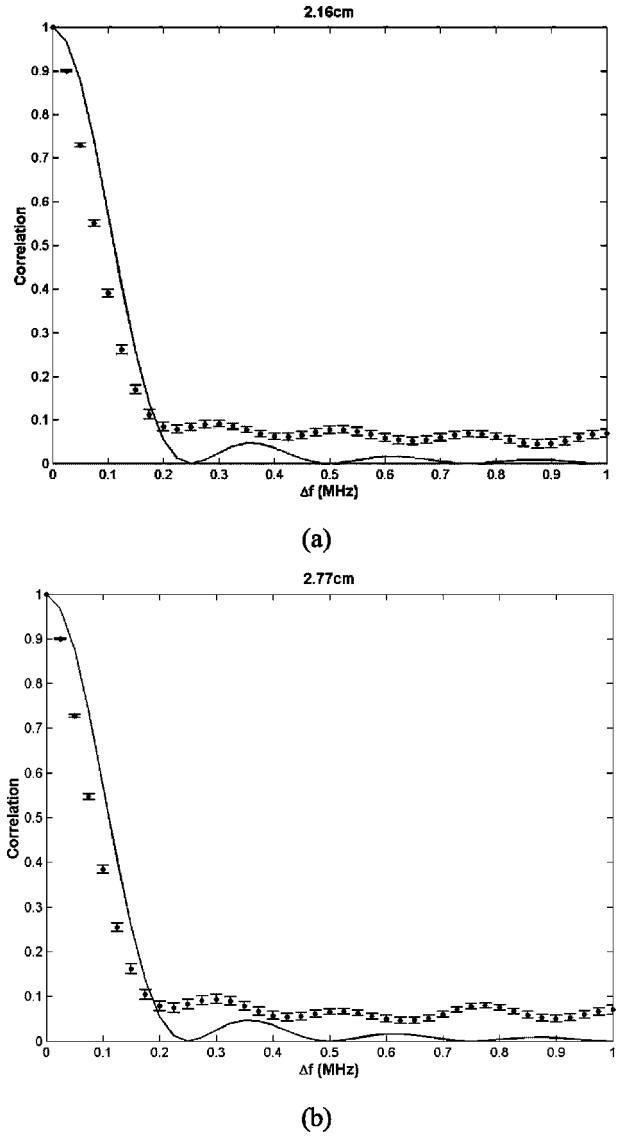

FIG. 4. Correlation between the attenuation versus frequency slope as a function of the increment between measurement frequencies for an echo data segment of length (a) 2.16 cm and (b) 2.77 cm. Solid lines are theoretical values, and dots with error bars are the results of phantom experiments.

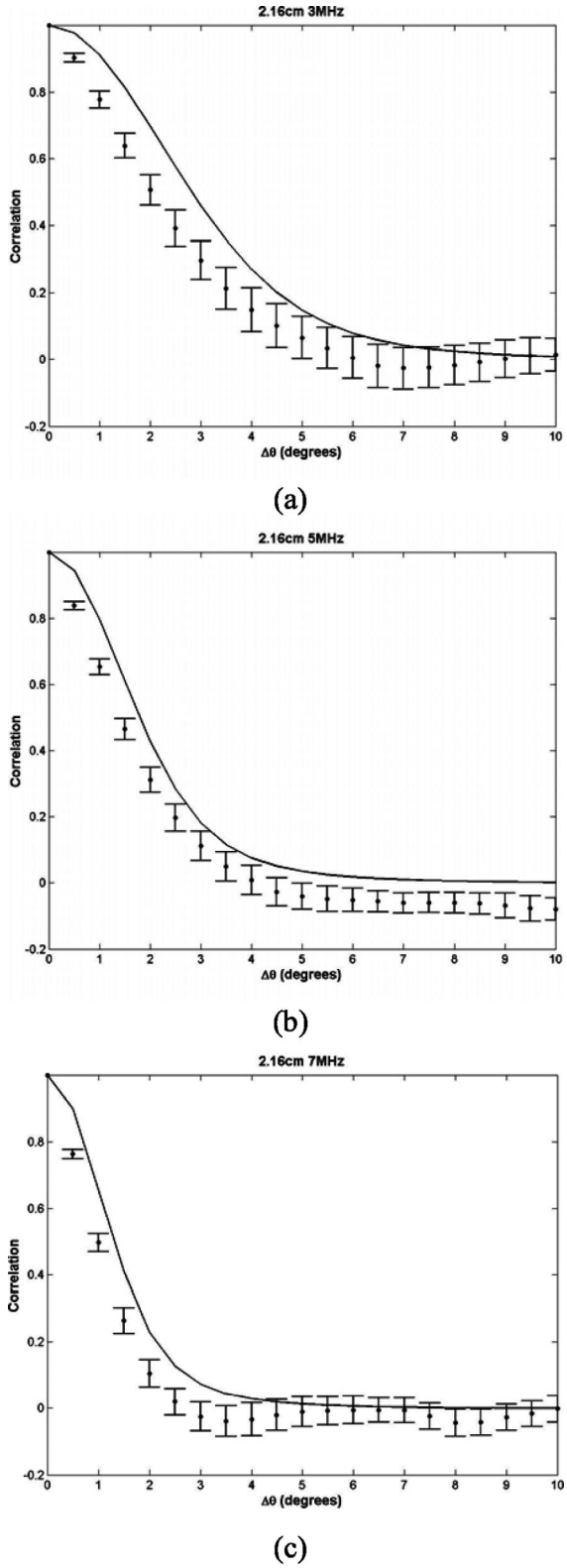

FIG. 5. Correlation between the attenuation versus frequency slope as a function of the angular separation between beam lines for a data segment of length 2.16 cm at frequencies of (a) 3 MHz, (b) 5 MHz, and (c) 7 MHz. Solid lines are theoretical values, and dots with error bars are the results of simulation experiments.

be simplified to Eq. (16). The assumption is generally good near the focal region of a transducer, although it may not represent the actual acoustic field at points away from the focus of a real transducer. However, during the design of a compounding scheme for any particular aperture and depth, a numerical calculation can be done using Eq. (10) with detailed knowledge of the acoustic field.

Our theoretical result is based on a model that a single acoustic line is rotated around a common center. Caution must be taken, therefore, on use of these results if multiple acoustic lines [$N_s \neq 1$ in Eq. (3)] are used to get an averaged spectrum before computing the attenuation. If spectra from several beam lines are averaged, the region in which scatterers contribute to the averaged spectrum will be wider than the region which contributes to the spectrum for a single acoustic line. Thus, the overlap between rotating acoustic fields will be larger in the averaged spectrum case than for the case where the spectrum is derived from rf data acquired over a single acoustic line if the angle rotated is the same. Therefore, the spectral decorrelation as a function of angular separation between beam lines will be slower when multiple acoustic lines are used to get an averaged spectrum, and so

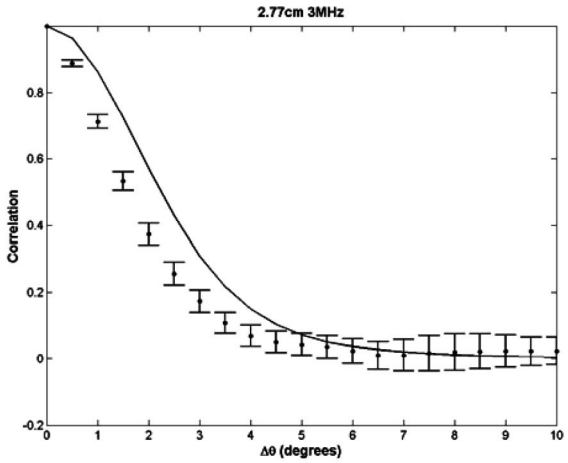

(a)

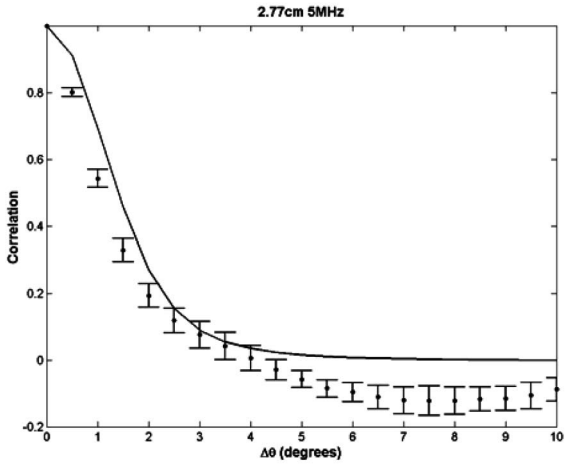

(b)

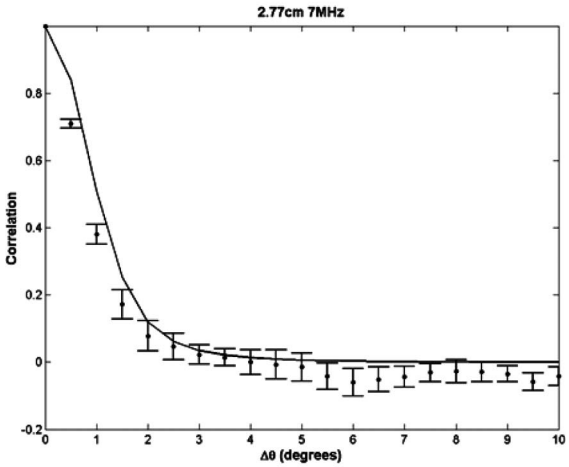

(c)

FIG. 6. Correlation between the attenuation versus frequency slope as a function of the angular separation between beam lines for a data segment of length 2.77 cm, at frequencies of (a) 3 MHz, (b) 5 MHz, and (c) 7 MHz. Solid lines are theoretical values, and dots with error bars are the results of simulation experiments.

will the attenuation decorrelation. Since frequency compounding does not have this effect when using averaged spectra from adjacent lines, it will have an advantage over spatial angular compounding in this case.

Our compounding algorithm is just one type of possible compounding methods that could be applied in attenuation estimations. Other approaches, for example, spectra compounding instead of parameter compounding, may be effective as well. For any real system, noise has to be incorporated into the model when considering an optimized compounding scheme. Still, this study sheds light on a path towards reliable local attenuation estimations. It is, in general, difficult to determine the dependencies of attenuation estimate correlations upon systematic parameters analytically. With simplified conditions such as those applied in the solution of our theoretical model, we are able to show the efficiency of angular or frequency compounding for different system parameters, such as the angular separation between compounded beam lines or the increment between compounded frequencies. With these relations, directions are given for choosing the best scheme for attenuation estimations with the smallest variance.

VI. CONCLUSION

Theoretical expressions for the correlation between attenuation versus frequency slope estimates generated for the same tissue location but using different frequency components or from different angles of incidence have been derived. Predicted results were compared with measurements from phantoms and with simulation data, respectively. Both predictions and measurement results show that the correlation between β estimates as a function of increment between measurement frequencies is independent of the length of the rf data segment over which the attenuation versus frequency slope is derived. However, it decreases with an increase in length of the gating window used in power spectra estimates. In contrast, the correlation between β estimates as a function of angular separation between beam lines does depend on the rf data segment length; it also depends on the frequency of the signal over which the attenuation versus frequency slope is computed. The higher the frequency and the longer the data segment, the faster the decorrelation will be. The relationships for correlation among β estimates can be used to optimize spatial angular and frequency compounding schemes in attenuation versus frequency slope measurements.

ACKNOWLEDGMENTS

This work was supported in part by NIH Grant Nos. R21EB002722 and R21EB003853.

APPENDIX A: CORRELATION BETWEEN PERIODOGRAM VALUES

The signal $V(t)$, gated by a window $p(t)$ with its center at t_0, is

$$V_g(t) = V(t)p(t-t_0). \tag{A1}$$

The value of its Fourier transform at frequency f_i is

$$V_g(f_i,t_0)=e^{-if_it_0}\int v(f)P(f_i-f)e^{ift_0}\,df, \tag{A2}$$

where $v(f)=\mathrm{FT}(V(t))$ and $P(f)=\mathrm{FT}(p(t))$.

At another frequency f_j, we have

$$V_g(f_j,t_0)=e^{-if_jt_0}\int v(f')P(f_j-f')e^{if't_0}\,df', \tag{A3}$$

Thus, the autocorrelation between the two Fourier transforms is

$$\rho=\langle V_g(f_i,t_0)V_g^*(f_j,t_0)\rangle\approx Ce^{-i(f_i-f_j)t_0}\mathrm{FT}(|p(t)|^2)_{\Delta f}. \tag{A4}$$

Here C is a constant absorbed into the normalization, $\Delta f=|f_j-f_i|$, $\langle ...\rangle$ means the expected value, and use is made of the fact that $p(t)$ and $P(f)$ are even functions.

Thus, the correlation between periodogram spectral estimates is

$$\rho(S_{f_i},S_{f_j})=|\rho|^2=|\mathrm{FT}(|p(t)|^2)_{\Delta f}|^2. \tag{A5}$$

APPENDIX B: ATTENUATION CORRELATIONS FOR DATA AT TWO ANGULAR POSITIONS

In our frequency compounding algorithm, the attenuation coefficients versus frequency slopes at angular positions θ_i and θ_j $(i\neq j)$ are given by

$$\beta_{\theta_i}=\frac{\Sigma_{k=1}^{n_f}\beta_{\theta_i}(f_k)}{n_f} \quad \text{and} \quad \beta_{\theta_j}=\frac{\Sigma_{k'=1}^{n_f}\beta_{\theta_j}(f_{k'})}{n_f}, \tag{B1}$$

where n_f is the number of frequency components used in frequency compounding. The variance of these two variables, $\mathrm{cov}(\beta_{\theta_i},\beta_{\theta_j})$, may be written as

$$\begin{aligned}\mathrm{cov}(\beta_{\theta_i},\beta_{\theta_j})&=\frac{1}{n_f^2}\mathrm{cov}\left(\sum_{k=1}^{n_f}\beta_{\theta_i}(f_k),\sum_{k'=1}^{n_f}\beta_{\theta_j}(f_{k'})\right)\\&=\frac{1}{n_f^2}\sum_{k=1}^{n_f}\mathrm{cov}(\beta_{\theta_i}(f_k),\beta_{\theta_j}(f_k)).\end{aligned} \tag{B2}$$

The second equal sign in Eq. (B2) is established because we assume that the covariance between β estimates made at two different angles is negligible unless those estimates are made at the same frequency, i.e., $\mathrm{cov}(\beta_{\theta_i}(f_k),\beta_{\theta_j}(f_{k'}))=0$ when $k'\neq k$. Using $\sigma_{\beta_{\theta_i}}=\sigma_{\beta_{\theta_j}}=\sigma_{\beta_\theta}=(1/N_f)\sqrt{\Sigma_{k=1}^{n_f}\sigma_{\beta_{f_k}}^2}=(\delta/n_f)\sqrt{\Sigma_{k=1}^{n_f}\sigma_{\beta_{f_k}}^2}$, in which σ_{β_θ} is the variance of the attenuation coefficient versus frequency slope estimate after frequency compounding but before spatial angular compounding, we write

$$\begin{aligned}\rho(\beta_{\theta_i},\beta_{\theta_j})&=\frac{\mathrm{cov}(\beta_{\theta_i},\beta_{\theta_j})}{\sigma_{\beta_{\theta_i}}\sigma_{\beta_{\theta_j}}}\\&=\frac{\Sigma_{k=1}^{n_f}\mathrm{cov}(\beta_{\theta_i}(f_k),\beta_{\theta_j}(f_k))}{\delta^2\Sigma_{k=1}^{n_f}\sigma_{\beta_{f_k}}^2}\\&=\frac{\Sigma_{k=1}^{n_f}\sigma_{\beta_{f_k}}^2\rho(\beta_{\theta_i}(f_k),\beta_{\theta_j}(f_k))}{\delta^2\Sigma_{k=1}^{n_f}\sigma_{\beta_{f_k}}^2}.\end{aligned} \tag{B3}$$

Since $\sigma_{\beta_{f_k}}=\sigma_{\alpha_{f_k}}/f_k$ and $\sigma_{\alpha_{f_k}}$ can be approximated as being independent of f_k [see Eq. (3) in the main text], we have

$$\rho(\beta_{\theta_i},\beta_{\theta_j})\approx\frac{\Sigma_{k=1}^{n_f}(1/f_k^2)\,\rho(\beta_{\theta_i}(f_k),\beta_{\theta_j}(f_k))}{\delta^2\Sigma_{k=1}^{n_f}(1/f_k^2)}. \tag{B4}$$

APPENDIX C: ATTENUATION CORRELATIONS RESULTING FROM CORRELATIONS IN POWER SPECTRA

The reference phantom method to derive β, the attenuation coefficient versus frequency slope, is carried out by applying a least squares algorithm to fit the log difference between a sample and a reference power spectral estimate at a given frequency versus the depth. The slope of this fit is proportional to the difference between the attenuation coefficient of the sample and that of the reference. With the known attenuation of the reference, the attenuation coefficient of the sample can be estimated. That value divided by the given frequency is the attenuation coefficient versus frequency slope, β.

Let β be the least squares slope fitted from the natural log difference between the sample and the reference power spectral estimate versus the depth, and let $\Delta\alpha$ be the difference between the attenuation coefficient of the sample and that of the reference at a chosen frequency:

$$\Delta\alpha=-b/4\times 8.68\ \ (\mathrm{dB/cm}). \tag{C1}$$

Here 8.68 is the conversion factor from nepers/cm to dB/cm. The correlation between the attenuation coefficient versus frequency slope, β, at positions 1 and 2 would be

$$\rho(\beta_1,\beta_2)=\rho(\alpha_1,\alpha_2)=\rho(b_1,b_2). \tag{C2}$$

Let x_m be the position of the mth independent power spectral estimate used to calculate the slope b at a specified frequency, and let Δ be the separation between these uniformly spaced data points. y_m is the mth value of the logged difference between the sample and reference power spectral estimates at different depths for that frequency. Thus $y_m=\ln S_m-\ln S_m^r=\ln RS_m$, where $(\mathrm{RS})_m$ is the ratio of the sample power spectrum to the reference power spectrum at point m. $m=1,...,n$, where n is the total number of independent power spectrum estimates along the data segment whose length is Z. In Fig. 3, the left panel depicts the situation described by Eq. (11), while the right panel corresponds to Eq. (12):

$$x_m=(m-1)\Delta+x_0. \tag{C3}$$

According to Bevington,[24]

$$b=\frac{1}{\Delta'}\left(n\sum x_m y_m-\sum x_m\sum y_m\right) \tag{C4}$$

in which $\Delta'=n\Sigma x_m^2-(\Sigma x_m)^2$. Inserting (C3) into (C4), we have

$$b=\frac{1}{\Delta'}n\Delta\sum_{m=1}^{n} a_m y_m, \tag{C5}$$

in which $a_m=m-n/2-1/2$ and $\Sigma_{m=1}^{n}a_m^2=(n-1)n(n+1)/12$.

Thus, we have

$$\begin{aligned}\mathrm{cov}(b_1,b_2)&=\frac{1}{\Delta'^2}n^2\Delta^2\mathrm{cov}\left(\sum_{u=1}^{n} a_{1u}y_{1u},\sum_{v=1}^{n} a_{2v}y_{2v}\right)\\&=\frac{1}{\Delta'^2}n^2\Delta^2\sum_{u=1}^{n}\sum_{v=1}^{n} a_{1u}a_{2v}\mathrm{cov}(y_{1u},y_{2v}).\end{aligned} \tag{C6}$$

It is reasonable to suppose that when $u\neq v$, covariance between y_u and y_v at two different positions 1, 2 is negligible, i.e., $\mathrm{cov}(y_{1u},y_{2v})=0$, when $1\neq 2$, and $u\neq v$. Also we have $\mathrm{cov}(y_{1u},y_{2v})=0$, when $1=2$, but $u\neq v$. The latter is because of the assumption that data points are independent. Thus, we have

$$\mathrm{cov}(b_1,b_2)=\frac{1}{\Delta'^2}n^2\Delta^2\sum_{m=1}^{n} a_m^2\mathrm{cov}(y_{1m},y_{2m}). \tag{C7}$$

Assume the following assumption holds for the error propagation from the ratio of the sample to reference power spectrum to its logged form,

$$\begin{aligned}\mathrm{cov}(y_{1m},y_{2m})&=\frac{\partial y_{1m}}{\partial \mathrm{RS}_{1m}}\frac{\partial y_{2m}}{\partial \mathrm{RS}_{2m}}\mathrm{cov}(\mathrm{RS}_{1m},\mathrm{RS}_{2m})\\&=\frac{1}{\mathrm{RS}_{1m}}\frac{1}{\mathrm{RS}_{2m}}\sigma_{\mathrm{RS}_{1m}}\sigma_{\mathrm{RS}_{2m}}\rho(\mathrm{RS}_{1m},\mathrm{RS}_{2m}).\end{aligned} \tag{C8}$$

And, from Ref. 25,

$$\begin{aligned}\sigma_{\mathrm{RS}_m}^2&=\left(\frac{\partial \mathrm{RS}_m}{\partial\overline{S_m^r}}\right)^2\mathrm{var}(\overline{S_m^r})+\left(\frac{\partial \mathrm{RS}_m}{\partial\overline{S_m}}\right)^2\mathrm{var}(\overline{S_m})\\&=\frac{N_S+N_r}{N_S N_r}\mathrm{RS}_m^2.\end{aligned} \tag{C9}$$

The relation $\mathrm{var}(S)=S^2$ is used in the above equation.[26] N_s and N_r represent the number of sample and reference waveforms used to calculate the spectra, respectively.

Combining Eqs. (C7)–(C9),

$$\mathrm{cov}(b_1,b_2)=\frac{N_s+N_r}{N_s N_r}\frac{1}{\Delta'^2}n^2\Delta^2\sum_{m=1}^{n} a_m^2\rho(\mathrm{RS}_{1m},\mathrm{RS}_{2m}). \tag{C10}$$

Assuming $\sigma_{y_m}=\sigma_y$ for all m, we have $\sigma_b^2=n\,\sigma_y^2/\Delta'$, so

$$\sigma_{b_1}\sigma_{b_2}=\frac{n}{\Delta'}\sigma_{y_1}\sigma_{y_2}. \tag{C11}$$

Similar to (C8) and (C9),

$$\sigma_{y_1}^2=\sigma_{y_2}^2=\sigma_y^2=\left(\frac{\partial y}{\partial \mathrm{RS}}\right)^2\sigma_{\mathrm{RS}}^2=\frac{N_s+N_r}{N_s N_r}. \tag{C12}$$

Combining (C2) and (C10)–(C12),

$$\rho(\beta_1,\beta_2)=\rho(b_1,b_2)=\frac{1}{\Delta'}n\Delta^2\sum_{m=1}^{n} a_m^2\rho(\mathrm{RS}_{1m},\mathrm{RS}_{2m}). \tag{C13}$$

Many reference signals are averaged to form the reference spectrum. Thus the variance of the reference spectrum can be deemed to be very small,

$$\rho(\mathrm{RS}_{1m},\mathrm{RS}_{2m})=\rho(S_{1m},S_{2m}) \tag{C14}$$

and

$$\Delta'=n\Sigma x_m^2-\left(\sum x_m\right)^2=n(n-1)\sigma_x^2=\frac{(n+1)n^2}{12(n-1)}Z^2. \tag{C15}$$

The last equality in Eq. (C15) was established because for n uniformly spaced points on a one-dimensional number axis spread over a distance of Z, $\sigma_x^2=[n(n+1)/12(n-1)^2]Z^2$. Notice that $Z=(n-1)\Delta$. Thus (C13) turns to

$$\rho(\beta_1,\beta_2)=\frac{12}{(n-1)n(n+1)}\sum_{m=1}^{n} a_m^2\rho(S_{1m},S_{2m}). \tag{C16}$$

[1] R. Kuc, "Clinical application of an ultrasound attenuation coefficient estimation technique for liver pathology characterization," IEEE Trans. Biomed. Eng. **27**, 312–319 (1980).

[2] Z. F. Lu, J. A. Zagzebski, and F. T. Lee, "Ultrasound backscatter and attenuation in human liver with diffuse disease," Ultrasound Med. Biol. **25**, 1047–1054 (1999).

[3] A. T. Stavros, D. Thickman, C. L. Rapp, M. A. Dennis, S. H. Parker, and G. A. Sisney, "Solid breast nodules: use of sonography to distinguish between benign and malignant lesions," Radiology **196**, 123–134 (1995).

[4] P. M. Lamb, N. M. Perry, S. J. Vinnicombe, and C. A. Wells, "Correlation between ultrasound characteristics, mammographic findings and histological grade in patients with invasive ductal carcinoma of the breast," Clin. Radiol. **55**, 40–44 (2000).

[5] J. G. Miller, J. E. Perez, J. G. Mottley, E. I. Madaras, P. H. Johnston, E. D. Blodgett, L. J. Thomas III, and B. E. Sobel, "Myocardial tissue characterization: an approach based on quantitative backscatter and attenuation," Proc.-IEEE Ultrason. Symp. **83**, 782–793 (1983).

[6] S. L. Bridal, P. Fornes, P. Bruneval, and G. Berger, "Parametric (intergrated backscatter and attenuation) images constructed using backscattered radio frequency signals (25-56 MHz) from human aorte in vitro," Ultrasound Med. Biol. **23**, 215–229 (1997).

[7] S. W. Flax, N. J. Pelc, G. H. Glover, F. D. Gutmann, and M. McLachlan, "Spectral Characterization and Attenuation Measurements in Ultrasound," Ultrason. Imaging **5**, 95–116 (1983).

[8] P. He and J. F. Greenleaf, "Application of stochastic-analysis to ultrasonic echoes—estimation of attenuation and tissue heterogeneity from peaks of echo envelope," J. Acoust. Soc. Am. **79**, 526–534 (1986).

[9] E. Walach, A. Shmulewitz, Y. Itzchak, and Z. Heyman, "Local tissue attenuation images based on pulse-echo ultrasound scans," IEEE Trans. Biomed. Eng. **36**, 211–221 (1989).

[10] B. S. Knipp, J. A. Zagzebski, T. A. Wilson, F. Dong, and E. L. Madsen, "Attenuation and backscatter estimation using video signal analysis applied to B-mode images," Ultrason. Imaging **19**, 221–233 (1997).

[11] R. Kuc and M. Schwartz, "Estimating the acoustic attenuation coefficient

slope for liver from reflected ultrasound signals,'' IEEE Trans. Sonics Ultrason. **SU-26**, 353–362 (1979).
[12] M. J. T. M. Cloostermans and J. M. Thijssen, ''A beam corrected estimation of the frequency dependent attenuation of biological tissues from backscattered ultrasound,'' Ultrason. Imaging **5**, 136–147 (1983).
[13] L. X. Yao, J. A. Zagzebski, and E. L. Madsen, ''Backscatter coefficient measurements using a reference phantom to extract depth-dependent instrumentation factors,'' Ultrason. Imaging **12**, 58–70 (1990).
[14] M. Fink, F. Hottier, and J. F. Cardoso, ''Ultrasonic signal processing for in vivo attenuation measurement: Short time Fourier analysis,'' Ultrason. Imaging **5**, 117–135 (1983).
[15] H. Tu, T. Varghese, E. L. Madsen, Q. Chen, and J. A. Zagzebski, ''Ultrasound attenuation imaging using compound acquistion and processing,'' Ultrason. Imaging **25**, 245–261 (2003).
[16] L. X. Yao, J. A. Zagzebski, and E. L. Madsen, ''Statistical uncertainty inultrasonic backscatter and attenuation coefficients determined with a reference phantom,'' Ultrasound Med. Biol. **17**, 187–194 (1991).
[17] R. F. Wagner, S. W. Smith, J. M. Sandrick, and H. Lopez, ''Statistics of speckle in ultrasound B-scans,'' IEEE Trans. Sonics Ultrason. **30**, 156–163 (1983).
[18] R. R. Entrekin, B. A. Porter, H. H. Sillesen, A. D. Wong, P. L. Cooperberg, and C. H. Fix, ''Real-time spatial compound imaging: application to breast, vascular, and musculoskeletal ultrasound,'' Semin Ultrasound CT MR **22**, 50–64 (2001).
[19] A. L. Gerig, T. Varghese, and J. A. Zagzebski, ''Improved parametric imaging of scatterer size estimates using angular compounding,'' IEEE Trans. Ultrason. Ferroelectr. Freq. Control **51**, 708–715 (2004).
[20] P. A. Magnin, O. T. von Ramm, and F. L. Thurstone, ''Frequency compounding for speckle contrast reduction in phased-array Images,'' Ultrason. Imaging **4**, 267–281 (1982).
[21] G. E. Trahey, J. W. Allison, S. W. Smith, and O. T. von Ramm, ''A quantitative approach to speckle reduction via frequency compounding,'' Ultrason. Imaging **8**, 151–164 (1986).
[22] M. O'Donnell and S. D. Silverstein, ''Optimum displacement for compound image generation in medical ultrasound,'' IEEE Trans. Ultrason. Ferroelectr. Freq. Control **35**, 470–476 (1988).
[23] A. L. Gerig, Q. Chen, and J. A. Zagzebski, ''Correlation of ultrasonic scatterer size estimates for the statistical analysis and optimization of angular compounding,'' J. Acoust. Soc. Am. **116**, 1832–1841 (2004).
[24] P. R. Bevington and D. K. Robinson, *Data Reduction and Error Analysis for the Physical Sciences*, 2nd ed. (McGraw-Hill, New York, 1992).
[25] A. L. Gerig, J. A. Zagzebski, and T. Varghese, ''Statistics of ultrasonic scatterer size estimation with a reference phantom,'' J. Acoust. Soc. Am. **113**, 3430–3437 (2002).
[26] P. Chaturvedi and M. F. Insana, ''Error bounds on ultrasonic scatter size estimates,'' J. Acoust. Soc. Am. **100**, 392–399 (1996).